Proceedings of the 2018 IEEE
International Conference on Robotics and Biomimetics
December 12-15, 2018, Kuala Lumpur, Malaysia

Comparisons among Six Numerical Methods for Solving Repetitive Motion Planning of Redundant Robot Manipulators*

1st Zhijun Zhang, Lingdong Kong, Ziyi Yan
School of Automation Science & Engineering
South China University of Technology
Guangzhou 510641, China
auzjzhang@scut.edu.cn; scutkld@foxmail.com; auzyyan@mail.scut.edu.cn

2nd Ke Chen
School of Electronic & Information Engineering
South China University of Technology
Guangzhou 510641, China
chenk@scut.edu.cn

3rd Shuai Li
Department of Computing
Hong Kong Polytechnic University
Hong Kong 999077, China
shuaili@polyu.edu.hk

4th Xilong Qu
School of Information Technology & Management
Hunan University of Finance and Economics
Changsha 410006, China
quxilong@126.com

5th Ning Tan
School of Data & Computer Science
Sun Yat-sen University
Guangzhou 510006, China
tann5@mail.sysu.edu.cn

***Abstract*—To ensure that each joint of redundant robot manipulators can return to its initial state when completes a closed-path tracking task, a repetitive motion planning (RMP) scheme is presented. On the basis of a quadratic programming (QP) framework, this RMP can be equivalently converted into a linear-variational-inequality (LVI) problem, and then into a piecewise linear projection equation (PLPE). In this paper, three novel numerical methods (i.e., M3, M5 and M6) and three traditional numerical methods (i.e., 94LVI, E47 and M4) are exploited, analyzed, and compared to solve PLPE, as well as RMP. The convergence of M5 method is theoretically proved, and that of M3 and M6 methods is analyzed by simulations. Moreover, comparative simulations of two complex path tracking tasks performed on a PUMA560 robot manipulator further verify the feasibility and effectiveness of the proposed numerical methods.**

***Index Terms*—Robot kinematics; Motion planning; Quadratic programming; Complex path tracking**

I. Introduction

Redundant robot manipulators contain extra degrees-of-freedom (DOF) than needed to complete a motion planning mission and thus have been researched widely in the past few decades [1], [2]. With more DOF, redundant robot manipulators possess abilities to complete complex tasks, such as collision-free planning [3], [4], singular configuration avoidance [5], [6], joint limit avoidance [2], [7], and planning cyclic motion while executing primary mission [1], [8], [9]. The fundamental problem of operations of redundant robot manipulators is the inverse kinematics [10]. However, there exists multiple-solution problem because the number of kinematical equations is less than the number of robot joint variables [11], [12]. The conventional approach to handle this redundancy problem is pseudo-inverse-based method [11], [12]. Nevertheless, if considering joint limits and joint-velocity limits, the redundancy problem is generally subjected to equalities, inequalities and other existing singularities. Unfortunately the aforementioned pseudo-inverse method is unsuitable to handle constraint problems described above [13].

Recently, a quadratic programming (QP) method is utilized popularly to solve the redundancy resolution problems of robot manipulators [14], [15]. On the basis of optimization theory, the QP-based method contains the ability to handle constraint problems. Therefore, the repetitive motion planning (RMP) of redundant robot manipulators, which constructed by equalities and inequalities, can be formulated under QP framework. According to [16], this QP-based RMP scheme can be converted into a linear-variational-inequality (LVI) problem, and further converted into a piecewise linear projection equation (PLPE). Hence the complex motion planning problem is alluded to equation solving problem which is relatively easy.

There are mainly two approaches to handle PLPE, as well as the original RMP, i.e., the neural network method [1], [2], [17]–[19] and the numerical method. In [19], a gradient neural network (GNN) which based on non-negative energy equations was proposed by Xia *et al.* to improve the effectiveness of computation for solving PLPE. In recent years, a Zhang neural network (ZNN) was proposed by Zhang *et al.* for solving time-varying problems subjected to equalities and inequalities [20]. Jin *et al.* utilized this Zhang neural dynamic method

This work supported in part by the National Natural Science Foundation under Grants 61603142 and 61633010, the Guangdong Foundation for Distinguished Young Scholars under Grant 2017A030306009, The Guangdong Youth Talent Support Program of Scientific and Technological Innovation under Grant 2017TQ04X475, the Science and Technology Program of Guangzhou under Grant 201707010225, the Fundamental Research Funds for Central Universities under Grant x2zdD2182410, the Scientific Research Starting Foundation of South China University of Technology, the National Key R&D Program of China under Grant 2017YFB1002505, the National Key Basic Research Program of China (973 Program) under Grant 2015CB351703, and the Guangdong Natural Science Foundation under Grant 2014A030312005.

978-1-7281-0377-8/18/$31.00 © 2018 IEEE

to solve joint-drift phenomenon of dual manipulators in [21]. Another approach is the numerical method [22]–[24]. Due to the iterative property, the computation time of numerical method is shorter than that of neural network method, and it is convenient to control robot manipulators on discrete computer and get pulse signal of drive motors. In [22] and [24], several numerical methods were presented by He *et al.* to solve PLPE. Another numerical method named 94LVI is proposed in [23] for solving QP problems subjected to bound constraints, and further applied to the motion planning of a planar robot manipulator. Zheng *et al.* compared three numerical methods (i.e., 94LVI, E47 and M4) for solving redundancy resolution problems in [25]. Moreover, the complete theorems of 94LVI and E47 methods to solve inequality constrained QP problems were presented in [16].

In this paper, inspired by previous researches, three novel numerical methods (i.e., M3, M5 and M6) and three traditional numerical methods (i.e., 94LVI, E47 and M4) are exploited, analyzed, and compared to solve the PLPE, as well as RMP, which is further applied to plan the repetitive motion of a PUMA560 manipulator. The remainder of this paper is organized as follows. Section II gives the problem formulation of the QP-based RMP for the redundant robot manipulators. The equivalent relationships among the RMP, the LVI, and the PLPE are theoretically analyzed in Section III. In Section IV, three novel numerical methods (i.e., M3, M5 and M6 methods) are proposed. Meanwhile, three traditional numerical methods (i.e., 94LVI, E47 and M4 methods) are also presented. In Section V, all the six numerical methods are exploited to solve RMP, and their solutions to a PUMA560 manipulator for tracking two complex closed-paths are performed by computer simulations. Finally, Section VI draws the conclusion and looks forward to future work.

The main contributions of this paper are listed as follows

- Three novel numerical methods (i.e., M3, M5 and M6) are proposed to solve repetitive motion planning of redundant robot manipulators.
- The global convergence property of M5 method is theoretically proved, and that of M3 and M6 methods is simulatively analyzed.
- Associating with three traditional methods (i.e., 94LVI, E47 and M4), the iterative algorithm of all the six numerical methods for solving repetitive motion planning is demonstrated.
- Two complex closed-path tracking experiments verify the feasibility and effectiveness of all the six numerical methods for solving RMP of redundant robot manipulators.

II. Problem Formulation

Consider the forward kinematics of robot manipulators, i.e.,

$$\mathcal{R} = \mathcal{F}(\theta) \tag{1}$$

where $\mathcal{R} \in \mathbb{R}^m$ denotes the position vector of end-effector; $\theta \in \mathbb{R}^n$ denotes the joint vector. Due to the nonlinearity and redundancy, it is difficult to obtained the solutions from (1) straightly. Thus we consider the first-order differential equation, i.e.,

$$\mathcal{J}(\theta)\dot{\theta} = \dot{\mathcal{R}} \tag{2}$$

where $\dot{\mathcal{R}} \in \mathbb{R}^m$ and $\dot{\theta} \in \mathbb{R}^n$ denote the end-effector velocity vector and the joint velocity vector, respectively; $\mathcal{J}(\theta) \in \mathbb{R}^{m\times n}$ is the Jacobian matrix. For a redundant manipulator, the dimension of end-effector cartesian space m is less than the dimension of the joint space n, hence the number of solutions to (1) and (2) is infinite.

The conventional approach to handle the multi-solutions problem is the pseudo-inverse method [26], i.e.,

$$\dot{\theta} = \mathcal{J}^{\dagger}(\theta)\dot{\mathcal{R}} + \xi\big(\mathcal{I} - \mathcal{J}^{\dagger}(\theta)\mathcal{J}(\theta)\big) \tag{3}$$

where $\mathcal{J}^{\dagger}(\theta) \in \mathbb{R}^{m\times n}$ denotes the generalized inverse of $\mathcal{J}(\theta)$; $\xi \in \mathbb{R}^n$ denotes an index for optimizing; term $(\mathcal{I} - \mathcal{J}^{\dagger}(\theta)\mathcal{J}(\theta))$ denotes the general solution to the homogeneous equation $\mathcal{J}(\theta)\dot{\theta} = 0$; $\mathcal{I}$ denotes the identity matrix.

However, the pseudo-inverse method (3) cannot solve the problem with inequalities, bound constraints and singularities [13]. In other words, the repetitive motion planning of the end-effector cannot be guaranteed by utilizing pseudo-inverse method. According to [14], [27], a QP framework which takes the drift-free criterion into consideration is proposed recently. This method requires each of the joint angle return to the initial state when finishing a closed-path tracking task. The drift-free criterion can be expressed as

$$(\dot{\theta} + \mathcal{C})^{\mathrm{T}}(\dot{\theta} + \mathcal{C})/2 \tag{4}$$

where $\mathcal{C} = \lambda(\theta(t) - \theta(0))$; $\lambda > 0$ is a coefficient designed to scale the magnitude of manipulator's response to the drift joint $\theta(t) - \theta(0)$. Combining repetitive motion planning with joint limits, the following QP-based minimization problem is obtained, i.e.,

$$\begin{aligned}
\text{min.}\quad & (\dot{\theta} + \mathcal{C})^{\mathrm{T}}(\dot{\theta} + \mathcal{C})/2 && (5)\\
\text{s.t.}\quad & \mathcal{J}(\theta)\dot{\theta} = \dot{\mathcal{R}} && (6)\\
& \theta^{-} \leqslant \theta \leqslant \theta^{+} && (7)\\
& \dot{\theta}^{-} \leqslant \dot{\theta} \leqslant \dot{\theta}^{+} && (8)
\end{aligned}$$

where θ^{+} and θ^{-} denote the upper/lower joint limits, respectively; $\dot{\theta}^{+}$ and $\dot{\theta}^{-}$ denote the upper/lower joint-velocity limits, respectively.

Based on [28], by utilizing an intensity coefficient $\upsilon > 0$, the dynamic constraint of joint-velocity can be obtained as

$$\upsilon(\theta^{-} - \theta) \leqslant \dot{\theta} \leqslant \upsilon(\theta^{+} - \theta) \tag{9}$$

where coefficient υ guarantees that the feasible region generated by constraint (8) is larger than that of constraint (9).

Remark 1. *Mathematically, coefficient υ is determined as $\upsilon \geqslant \max_{1\leqslant i\leqslant n} = \{(\dot{\theta}_i^{+} - \dot{\theta}_i^{-})/(\theta_i^{+} - \theta_i^{-})\}$, and the feasible regions of (8) and (9) can be combined as*

$$\zeta^{-} \leqslant \dot{\theta} \leqslant \zeta^{+} \tag{10}$$

where $\zeta_i^- = \max\{\dot\theta_i^-, \upsilon(\theta_i^- - \theta_i)\}$*;* $\zeta_i^+ = \min\{\dot\theta_i^+, \upsilon(\theta_i^+ - \theta_i)\}$*;* i *denotes the* i*-th joint.*

Proof: The dynamic constraint (9) restrains joint-velocity $\dot\theta$ by considering current joint θ and its upper/lower joint limits θ^+ and θ^-. There exists two cases.

- Caes 1: When joint θ increases/decreases and tends to its upper/lower joint limits, the upper/lower bounds of dynamic constraint (9) will tend to zero. In other words, the joint-velocity $\dot\theta$ will tend to zero and manipulators will stop moving.
- Caes 2: When joint θ reaches its upper/lower joint limits, the upper/lower bounds of dynamic constraint (9) are $\dot\theta \leq 0$ and $\dot\theta \geq 0$, respectively. In other words, joint θ will not increase/decrease anymore. Therefore, θ will never exceed its secure limit. ■

In conclusion, the RMP of redundant robot manipulators can described be as follows

$$\text{min.} \quad \dot\theta^{\mathrm{T}}\mathcal{I}\dot\theta/2 + \mathcal{C}^{\mathrm{T}}\dot\theta \tag{11}$$

$$\text{s.t.} \quad \mathcal{J}(\theta)\dot\theta = \dot{\mathcal{R}} \tag{12}$$

$$\zeta^- \leqslant \dot\theta \leqslant \zeta^+ \tag{13}$$

Moreover, on the basis of dual decision theorem [29], the dual form of RMP (11)-(13) is

$$\text{max.} \quad -\dot\theta^{\mathrm{T}}\mathcal{I}\dot\theta/2 + \Im^{\mathrm{T}}\dot{\mathcal{R}} + \wp^{-\mathrm{T}}\zeta^- - \wp^{+\mathrm{T}}\zeta^+ \tag{14}$$

$$\text{s.t.} \quad \mathcal{I}\dot\theta + \mathcal{C} = \mathcal{J}^{\mathrm{T}}(\theta)\Im + \wp^- - \wp^+ \tag{15}$$

$$\Im \text{ arbitrary}, \wp^- \geq 0, \wp^+ \geq 0 \tag{16}$$

where dual decision variable $\Im$ satisfies equality constraint (12); dual decision variables $\wp^-$ and $\wp^+$ satisfy inequality constraint (13).

III. Equivalent Theorems

In this section, two theorems are proposed to demonstrate the equivalent relationships among the repetitive motion planning (RMP), the linear-variational-inequality (LVI) problem, and the piecewise linear projection equation (PLPE).

Theorem 1. *(Equivalence between RMP and LVI) Suppose that there exists an optimal solution* $\theta^* \in \mathbb{R}^n$ *to RMP (11)-(13). Then RMP (11)-(13) is equivalent to a LVI problem which is to find a vector* $\mathcal{U}^* \in \Omega = \{\mathcal{U} \mid \mathcal{U}^- \leqslant \mathcal{U} \leqslant \mathcal{U}^+\} \subset \mathbb{R}^{n+m}$ *such that*

$$(\mathcal{U} - \mathcal{U}^*)^T(\mathcal{M}\mathcal{U}^* + q) \geqslant 0, \quad \forall\, \mathcal{U} \in \Omega \tag{17}$$

where the primal-dual vector $\mathcal{U} \in \mathbb{R}^{n+m}$ *and the upper/lower bounds* $\mathcal{U}^+$*,* $\mathcal{U}^- \in \mathbb{R}^{n+m}$ *are respectively defined as*

$$\mathcal{U} = \begin{bmatrix} \dot\theta \\ \Im \end{bmatrix}, \ \mathcal{U}^+ = \begin{bmatrix} \zeta^+ \\ \omega l \end{bmatrix}, \ \mathcal{U}^- = \begin{bmatrix} \zeta^- \\ -\omega l \end{bmatrix} \in \mathbb{R}^{n+m}. \tag{18}$$

In (18), $l := [1, ..., 1]^T$ *denotes a m-dimensional vector whose elements are positive integer* 1*, and* $\omega >> 0 \in \mathbb{R}^m$ *is defined to replace* $+\infty$ *numerically. Coefficient matrix* $\mathcal{M}$ *and vector* q *are respectively defined as*

$$\begin{aligned} \mathcal{M} &= \begin{bmatrix} \mathcal{I} & -\mathcal{J}^T \\ \mathcal{J} & 0 \end{bmatrix} \in \mathbb{R}^{(n+m)\times(n+m)} \\ q &= \begin{bmatrix} \mathcal{C} \\ -\dot{\mathcal{R}} \end{bmatrix} \in \mathbb{R}^{n+m}. \end{aligned} \tag{19}$$

Proof: See Theorem 1 in [16]. ■

Theorem 2. *(Equivalence between LVI and PLPE) Suppose there exists an optimal solution* $\dot\theta^* \in \mathbb{R}^n$ *to RMP (11)-(13), LVI problem (17) is equivalent to the following PLPE*

$$\mathcal{P}_\Omega\big(\mathcal{U} - (\mathcal{M}\mathcal{U} + q)\big) - \mathcal{U} = 0 \tag{20}$$

where $\mathcal{P}_\Omega(\cdot) : \mathbb{R}^{n+m} \to \Omega$ *is a piecewise-linear projection operator, with the* i*-th element defined as*

$$\big(\mathcal{P}_\Omega(\mathcal{U})\big)_i = \begin{cases} \mathcal{U}_i^-, & if \ \ \mathcal{U}_i < \mathcal{U}_i^- \\ \mathcal{U}_i, & if \ \ \mathcal{U}_i^- \leqslant \mathcal{U}_i \leqslant \mathcal{U}_i^+ \\ \mathcal{U}_i^+, & if \ \ \mathcal{U}_i > \mathcal{U}_i^- \end{cases}$$

where $i = 1, 2, ..., n+m$*;* $\mathcal{M}$*,* $\mathcal{U}$*, and* q *are defined as the same to (18) and (19).*

Proof: See Theorem 2 in [16]. ■

IV. Numerical Methods

In this section, three traditional numerical methods (i.e., 94LVI, E47, and M4) in [24], [25] and three novel numerical methods (i.e., M3, M5 and M6) are introduced to solve PLPE (20), as well as the original RMP (11)-(13). Furthermore, the upper bound of numerical sequence is theoretically analyzed, and the global convergence property of M5 method is sincerely proved.

A. Iterative Algorithm

Note that the iterative equation of numerical methods is

$$\mathcal{U}^{k+1} = \mathcal{U}^k - \rho(\mathcal{U}^k)\mathcal{Q}e(\mathcal{U}^k). \tag{21}$$

With different step length $\rho(\mathcal{U}^k)$ and matrix $\mathcal{Q}$, the following six numerical methods can be obtained.

★ **94LVI method:**
For symmetric $\mathcal{M} \geq 0$,

$$\mathcal{Q} = \mathcal{I}, \qquad \rho(\mathcal{U}^k) = \frac{\|e(\mathcal{U}^k)\|_2^2}{e(\mathcal{U}^k)^{\mathrm{T}}(\mathcal{I} + \mathcal{M})e(\mathcal{U}^k)}. \tag{22}$$

★ **E47 method:**
For symmetric $\mathcal{M} > 0$,

$$\mathcal{Q} = \mathcal{M}^{-1}, \qquad \rho(\mathcal{U}^k) = \frac{\|e(\mathcal{U}^k)\|_2^2}{e(\mathcal{U}^k)^{\mathrm{T}}(\mathcal{I} + \mathcal{M}^{-1})e(\mathcal{U}^k)}. \tag{23}$$

★ **M3 method:**
For symmetric $\mathcal{M} > 0$,

$$\mathcal{Q} = \mathcal{I} + \mathcal{M}^{-1}, \quad \rho(\mathcal{U}^k) = \frac{\|e(\mathcal{U}^k)\|_2^2}{\|(\mathcal{I} + \mathcal{M}^{-1})e(\mathcal{U})\|_{\mathcal{I}+\mathcal{M}}^2}. \tag{24}$$

★ **M4 method:**
For $\mathcal{M} > 0$ but not necessarily symmetric,

$$\mathcal{Q} = (\mathcal{I} + \mathcal{M})^{-1}, \qquad \rho(\mathcal{U}^k) = 1. \tag{25}$$

★ **M5 method:**
For $\mathcal{M} > 0$ but not necessarily symmetric,

$$\mathcal{Q} = \mathcal{M}^{\mathrm{T}}, \qquad \rho(\mathcal{U}^k) = \frac{\|e(\mathcal{U}^k)\|_2^2}{\|e(\mathcal{U})\|_{\mathcal{M}(\mathcal{I}+\mathcal{M}^{\mathrm{T}})}^2}. \tag{26}$$

★ **M6 method:**

For $\mathcal{M} > 0$ but not necessarily symmetric,

$$\mathcal{Q} = \mathcal{I} + \mathcal{M}^{-1}, \qquad \rho(\mathcal{U}^k) = \frac{\|e(\mathcal{U}^k)\|_2^2}{\|e(\mathcal{U})\|^2_{\mathcal{M}(\mathcal{I}+\mathcal{M}^{\mathrm{T}})}}. \tag{27}$$

In conclusion, the iterative algorithm for solving PLPE (20) as well as the original RMP (11)-(13) can be obtained as Algorithm 1.

Algorithm 1 Iterative Algorithm of RMP (11)-(13)

```
Require:
    coefficients $\mathcal{I}$, $\mathcal{C}$, $\dot{\mathcal{R}}$, $\zeta^-$, $\zeta^+$, initial value $\dot{\theta}(0)$;
Ensure:
    optimal solution $\dot{\theta}^*$;
1: Generate $\mathcal{M}$, $q$, $\mathcal{U}^+$, $\mathcal{U}^-$ via (17) and (18);
2: Set $k = 0$, generate $\mathcal{U}^0$ from $\dot{\theta}(0)$ via (17);
3: Compute $e(\mathcal{U}^k)$. If $\mathcal{U}^k \in \Omega^*$ [i.e., theoretically $e(\mathcal{U}^k) = 0$, but practically $\|e(\mathcal{U}^k)\|_2 \le 10^{-3}$], then go to Step 6. Otherwise, go to Step 4;
4: Compute
       ⋆ for 94LVI method, generate $\mathcal{Q}$ and $\rho(\mathcal{U}^k)$ via (22);
       ⋆ for E47 method, generate $\mathcal{Q}$ and $\rho(\mathcal{U}^k)$ via (23);
       ⋆ for M3 method, generate $\mathcal{Q}$ and $\rho(\mathcal{U}^k)$ via (24);
       ⋆ for M4 method, generate $\mathcal{Q}$ and $\rho(\mathcal{U}^k)$ via (25);
       ⋆ for M5 method, generate $\mathcal{Q}$ and $\rho(\mathcal{U}^k)$ via (26);
       ⋆ for M6 method, generate $\mathcal{Q}$ and $\rho(\mathcal{U}^k)$ via (27);
         ▶ $\mathcal{U}^{k+1} = \mathcal{U}^k - \rho(\mathcal{U}^k)\mathcal{Q}e(\mathcal{U}^k)$;
5: Increase $k$ by one, go to Step 2;
6: Output $\dot{\theta}^*$ which is consisted by the first $n$ elements of $\mathcal{U}^k$;
```

B. Theoretical Analysis

Theorem 3. *(Sequence Theorem)*

For $\forall\, \mathcal{U} \in \Omega$, sequence $\{\mathcal{U}^k\}$ generated by each method of all the above six numerical methods (22)-(27) for solving PLPE (20) satisfies

$$\|\mathcal{U}^{k+1} - \mathcal{U}^*\|_{\mathcal{G}}^2 \le \|\mathcal{U}^k - \mathcal{U}^*\|_{\mathcal{G}}^2 - \rho(\mathcal{U}^k)\|e(\mathcal{U}^k)\|_2^2 \tag{28}$$

where $\mathcal{G} = \mathcal{I} + (\mathcal{M}^T)^{-1}$.

Proof: Firstly, the iterative error function of PLPE (20) is defined as

$$e(\mathcal{U}^k) = \mathcal{U}^k - \mathcal{P}_\Omega\big(\mathcal{U}^k - (\mathcal{M}\mathcal{U}^k + q)\big). \tag{29}$$

Considering the following relationship

$$\begin{aligned} \|\mathcal{U}^{k+1} - \mathcal{U}^*\|_{\mathcal{G}}^2 &= \|(\mathcal{U}^k - \mathcal{U}^*) - \rho(\mathcal{U}^k)\mathcal{Q}e(\mathcal{U}^k)\|_{\mathcal{G}}^2 \\ &= \|\mathcal{U}^k - \mathcal{U}^*\|_{\mathcal{G}}^2 - 2\rho(\mathcal{U}^k)(\mathcal{U}^k - \mathcal{U}^*)^{\mathrm{T}}\mathcal{G}\mathcal{Q}e(\mathcal{U}^k) \\ &\quad + \rho^2(\mathcal{U}^k)e(\mathcal{U}^k)^{\mathrm{T}}\mathcal{Q}^{\mathrm{T}}\mathcal{G}\mathcal{Q}e(\mathcal{U}^k) \end{aligned} \tag{30}$$

where $\rho(\mathcal{U}^k)e(\mathcal{U}^k)^{\mathrm{T}}\mathcal{Q}^{\mathrm{T}}\mathcal{G}\mathcal{Q}e(\mathcal{U}^k) = \|e(\mathcal{U}^k)\|_2^2$ and $\mathcal{G}\mathcal{Q} = \mathcal{I} + \mathcal{M}^{\mathrm{T}}$.

Eq. (30) can be rewritten as

$$\begin{aligned} \|\mathcal{U}^{k+1} - \mathcal{U}^*\|_{\mathcal{G}}^2 = \;& \|\mathcal{U}^k - \mathcal{U}^*\|_{\mathcal{G}}^2 + \rho(\mathcal{U}^k)\|e(\mathcal{U}^k)\|_2^2 \\ & -2\rho(\mathcal{U}^k)(\mathcal{U}^k - \mathcal{U}^*)^{\mathrm{T}}(\mathcal{I} + \mathcal{M}^{\mathrm{T}})e(\mathcal{U}^k). \end{aligned}$$

Based on projection property in [30], we have

$$\big(\upsilon - \mathcal{P}_\Omega(\upsilon)\big)^{\mathrm{T}}\big(\mathcal{P}_\Omega(\upsilon) - \gamma\big) \ge 0, \quad \upsilon \in \mathbb{R}. \tag{31}$$

By setting $\upsilon = \mathcal{U}^k - (\mathcal{M}\mathcal{U}^k + q)$, $\gamma = \mathcal{U}^*$, and in view of (29), the following inequality can be obtained, i.e.,

$$\big(\mathcal{P}_\Omega(\mathcal{U}^k - (\mathcal{M}\mathcal{U}^k + q) - \mathcal{U}^*)\big)^{\mathrm{T}}\big(e(\mathcal{U}^k) - (\mathcal{M}\mathcal{U}^k + q)\big) \ge 0.$$

It follows from the above that

$$\begin{aligned} &\big(\mathcal{P}_\Omega(\mathcal{U}^k - (\mathcal{M}\mathcal{U}^k + q) - \mathcal{U}^*)\big)^{\mathrm{T}} e(\mathcal{U}^k) \\ &\qquad \ge \big(\mathcal{P}_\Omega(\mathcal{U}^k - (\mathcal{M}\mathcal{U}^k + q) - \mathcal{U}^*)\big)^{\mathrm{T}}(\mathcal{M}\mathcal{U}^k + q) \end{aligned}$$

and then

$$\begin{aligned} &\big(\mathcal{U}^k - e(\mathcal{U}^k) - \mathcal{U}^*\big)^{\mathrm{T}} e(\mathcal{U}^k) \ge \\ &\qquad \big(\mathcal{P}_\Omega(\mathcal{U}^k - (\mathcal{M}\mathcal{U}^k + q) - \mathcal{U}^*)\big)^{\mathrm{T}}(\mathcal{M}\mathcal{U}^k + q), \end{aligned}$$

and thus

$$\begin{aligned} &(\mathcal{U}^k - \mathcal{U}^*)^{\mathrm{T}} e(\mathcal{U}^k) \ge \|e(\mathcal{U}^k)\|_2^2 \\ &\quad + \big(\mathcal{P}_\Omega(\mathcal{U}^k - (\mathcal{M}\mathcal{U}^k + q) - \mathcal{U}^*)\big)^{\mathrm{T}}(\mathcal{M}\mathcal{U}^k + q). \end{aligned} \tag{32}$$

Also note that

$$\begin{aligned} &(\mathcal{U}^k - \mathcal{U}^*)^{\mathrm{T}}\mathcal{M}^{\mathrm{T}} e(\mathcal{U}^k) \\ &\quad = e(\mathcal{U}^k)^{\mathrm{T}}(\mathcal{M}\mathcal{U}^k + q) - e(\mathcal{U}^k)^{\mathrm{T}}(\mathcal{M}\mathcal{U}^* + q). \end{aligned} \tag{33}$$

Combining (32) and (33), we have

$$\begin{aligned} &(\mathcal{U}^k - \mathcal{U}^*)^{\mathrm{T}}(\mathcal{I} + \mathcal{M}^{\mathrm{T}})e(u^k) \ge \|e(\mathcal{U}^k)\|_2^2 \\ &\quad + (\mathcal{U}^k - \mathcal{U}^*)^{\mathrm{T}}(\mathcal{M}\mathcal{U}^k + q) - e(\mathcal{U}^k)^{\mathrm{T}}(\mathcal{M}\mathcal{U}^* + q) \\ &= \|e(\mathcal{U}^k)\|_2^2 + (\mathcal{U}^k - \mathcal{U}^*)^{\mathrm{T}}(\mathcal{M}\mathcal{U}^k + q) \\ &\quad - \big(\mathcal{U}^* - \mathcal{P}_\Omega(\mathcal{U}^k - (\mathcal{M}\mathcal{U}^k + q))\big)^{\mathrm{T}}(\mathcal{M}\mathcal{U}^* + q) \\ &\quad - (\mathcal{U}^k - \mathcal{U}^*)^{\mathrm{T}}(\mathcal{M}\mathcal{U}^* + q) \\ &= \|e(\mathcal{U}^k)\|_2^2 + \big(\mathcal{P}_\Omega(\mathcal{U}^k - (\mathcal{M}\mathcal{U}^k + q)) - \mathcal{U}^*\big)^{\mathrm{T}}(\mathcal{M}\mathcal{U}^* + q) \\ &\quad + (\mathcal{U}^k - \mathcal{U}^*)^{\mathrm{T}}\mathcal{M}(\mathcal{U}^k - \mathcal{U}^*) \\ &\ge \|e(\mathcal{U}^k)\|_2^2 \\ &\quad + \big(\mathcal{P}_\Omega(\mathcal{U}^k - (\mathcal{M}\mathcal{U}^k + q)) - u^*\big)^{\mathrm{T}}(\mathcal{M}\mathcal{U}^* + q). \end{aligned} \tag{34}$$

By setting $\upsilon = \mathcal{U}^* - (\mathcal{M}\mathcal{U}^* + q)$ and $\gamma = \mathcal{P}_\Omega\big(\mathcal{U}^k - (\mathcal{M}\mathcal{U}^k + q)\big)$, in view of $\mathcal{U}^* = \mathcal{P}_\Omega\big(\mathcal{U}^* - (\mathcal{M}\mathcal{U}^* + q)\big)$, it follows from projection property (31) that

$$\big(\mathcal{P}_\Omega(\mathcal{U}^k - (\mathcal{M}\mathcal{U}^k + q)) - \mathcal{U}^*\big)^{\mathrm{T}}(\mathcal{M}\mathcal{U}^* + q) \ge 0 \tag{35}$$

and thus (34) yields

$$(\mathcal{U}^k - \mathcal{U}^*)^{\mathrm{T}}(\mathcal{I} + \mathcal{M}^{\mathrm{T}})e(\mathcal{U}^k) \ge \|e(\mathcal{U}^k)\|_2^2. \tag{36}$$

Considering (31) and (36) together, then the following relationship holds true, i.e.,

$$\begin{aligned} \|\mathcal{U}^{k+1} - \mathcal{U}^*\|_{\mathcal{G}}^2 &\le \|\mathcal{U}^k - \mathcal{U}^*\|_{\mathcal{G}}^2 \\ &\quad - 2\rho(\mathcal{U}^k)\|e(\mathcal{U}^k)\|_2^2 + \rho(\mathcal{U}^k)\|e(\mathcal{U}^k)\|_2^2 \\ &\le \|\mathcal{U}^k - \mathcal{U}^*\|_{\mathcal{G}}^2 - \rho(\mathcal{U}^k)\|e(\mathcal{U}^k)\|_2^2. \end{aligned}$$

Therefore, the sequence $\{\mathcal{U}^k\}$ generated by all the six numerical methods (22)-(27) for solving PLPE (20) satisfies

$$\|\mathcal{U}^{k+1} - \mathcal{U}^*\|_{\mathcal{G}}^2 \le \|\mathcal{U}^k - \mathcal{U}^*\|_{\mathcal{G}}^2 - \rho(\mathcal{U}^k)\|e(\mathcal{U}^k)\|_2^2 \tag{37}$$

and the proof is thus complete. ■

Theorem 4. *(Convergence Theorem)*
For $\forall\, \mathcal{U} \in \Omega$, sequence $\{\mathcal{U}^k\}$ generated by M5 method (26) converges to an optimal solution $u^* \in \Omega^*$ to PLPE (20), with its first n elements consisting the optimal solution to RMP (11)-(13).

Proof: Firstly, note that $\rho(\mathcal{U}^k)$ is bounded below in (26). Therefore, there exits a sufficiently small constant $\sigma > 0$, and it follows from Theorem 3 that

$$\sigma \|e(\mathcal{U}^k)\|_2^2 \le \|\mathcal{U}^k - \mathcal{U}^*\|_{\mathcal{G}}^2 - \|\mathcal{U}^{k+1} - \mathcal{U}^*\|_{\mathcal{G}}^2, \forall\, \mathcal{U}^* \in \Omega \quad (38)$$

with $k = 0, 1, 2, 3, ...$, we have

$$\begin{gathered}
\sigma \|e(\mathcal{U}^0)\|_2^2 \le \|\mathcal{U}^0 - \mathcal{U}^*\|_{\mathcal{G}}^2 - \|\mathcal{U}^1 - \mathcal{U}^*\|_{\mathcal{G}}^2 \\
\sigma \|e(\mathcal{U}^1)\|_2^2 \le \|\mathcal{U}^1 - \mathcal{U}^*\|_{\mathcal{G}}^2 - \|\mathcal{U}^2 - \mathcal{U}^*\|_{\mathcal{G}}^2 \\
\sigma \|e(\mathcal{U}^2)\|_2^2 \le \|\mathcal{U}^2 - \mathcal{U}^*\|_{\mathcal{G}}^2 - \|\mathcal{U}^3 - \mathcal{U}^*\|_{\mathcal{G}}^2 \\
\vdots \\
\sigma \|e(\mathcal{U}^j)\|_2^2 \le \|\mathcal{U}^j - \mathcal{U}^*\|_{\mathcal{G}}^2 - \|\mathcal{U}^{j+1} - \mathcal{U}^*\|_{\mathcal{G}}^2 \\
\vdots
\end{gathered}$$

Adding up all the inequalities above leads to the following result, i.e.,

$$\begin{aligned}
\sigma \sum_{k=0}^{+\infty} \|e(\mathcal{U}^k)\|_2^2 &\le \|\mathcal{U}^0 - \mathcal{U}^*\|_{\mathcal{G}}^2 - \lim_{j\to\infty} \|\mathcal{U}^{j+1} - \mathcal{U}^*\|_{\mathcal{G}}^2 \\
&\le \|\mathcal{U}^0 - \mathcal{U}^*\|_{\mathcal{G}}^2
\end{aligned} \quad (39)$$

which can be rewritten as

$$\sum_{k=0}^{+\infty} \|e(\mathcal{U}^k)\|_2^2 \le \frac{\|\mathcal{U}^0 - \mathcal{U}^*\|_{\mathcal{G}}^2}{\sigma} < +\infty. \quad (40)$$

Hence, there exits a positive value $\alpha \in [0, \|\mathcal{U}^0 - \mathcal{U}^*\|_{\mathcal{G}}^2/\sigma]$ satisfies

$$\lim_{g\to\infty} \sum_{k=0}^{g} \|e(\mathcal{U}^k)\|_2^2 = \alpha. \quad (41)$$

According to the definition of series convergence, summation sequence $\lim_{g\to\infty} \sum_{k=0}^{g} \|e(\mathcal{U}^k)\|_2^2$ is convergent, and thus

$$\lim_{k\to\infty} \|e(\mathcal{U}^k)\|_2^2 = 0 \quad (42)$$

i.e.,

$$\lim_{k\to\infty} e(\mathcal{U}^k) = 0. \quad (43)$$

With $\mathcal{U}^* \in \Omega^*$ denoting an optimal solution to PLPE (20) as well as LVI problem (17), and in view of $\lim_{k\to\infty} \|e(\mathcal{U}^k)\|_2^2 = \lim_{k\to\infty} \|\mathcal{U}^k - \mathcal{U}^*\|_2^2 = 0$, we can draw the conclusion that $e(\mathcal{U}^*) = 0$ and $\lim_{k\to\infty} \mathcal{U}^k = \mathcal{U}^*$.

Based on the definition of $\mathcal{U}$, for RMP (11)-(13), we know that $\dot{\theta}^*$ constitutes the first n elements of $\mathcal{U}^*$. According to the definition of two-norm, we have

$$\|\mathcal{U}^k - \mathcal{U}^*\|_2^2 = \|\dot{\theta}^k - \dot{\theta}^*\|_2^2 + \|\Im^k - \Im^*\|_2^2. \quad (44)$$

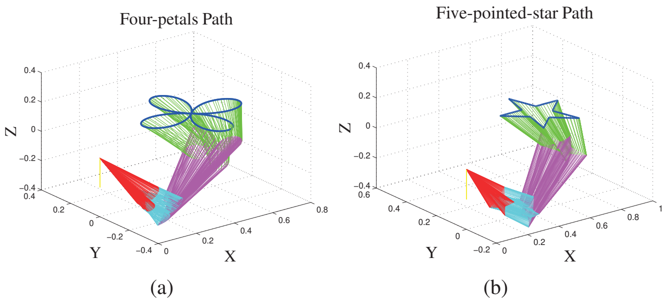

Fig. 1. Two complex tracking paths in simulation. (a) Four-petals path. (b) Five-pointed-star path.

TABLE I
JOINT LIMITS (RAD) OF PUMA560 MANIPULATOR

Joint	1	2	3	4	5	6
θ^+	2.7751	0.7504	3.1415	2.9671	0.0349	3.1416
θ^-	-2.7751	-3.1416	-0.9058	-1.9199	-1.7453	-3.1416

For (44), with $\|\cdot\|_2^2 \ge 0$, we can draw the conclusion that $\lim_{k\to\infty} \|\dot{\theta}^k - \dot{\theta}^*\|_2^2 = 0$. Thus $\lim_{k\to\infty} \dot{\theta}^k = \dot{\theta}^*$, that is to say, the first n elements of $\mathcal{U}^*$ constitute the optimal solution $\dot{\theta}^*$ to RMP (11)-(13). The proof is thus complete. ■

Remark 2. *The global convergence properties of 94LVI, E47 and M4 are theoretically proved in [24], and of M3 and M6 are synthesized from experiment results.*

V. SIMULATIVE EXPERIMENTS

In this section, simulative experiments for solving RMP (11)-(13) are performed to verify the effectiveness of three proposed methods, i.e., M3, M5 and M6. For comparison, the results of traditional 94LVI, E47 and M4 methods are also presented.

The simulative experiments are performed on a PUMA560 robot manipulator (6-DOF), whose initial state is defined as $\theta(0) = [0; -\pi/4; 0; \pi/2; -\pi/4; 0]$ (rad), and joint-velocity limits are $[-1.5, 1.5]$ (rad/s). The joint limits of PUMA560 manipulator are shown in Table I.

Two complex closed-paths (as shown in Fig. 1) are introduced to the experiments. The manipulator is expected to perform a drift-free repetitive motion, i.e., every joint of this manipulator can return to the initial state after completing a whole cyclic motion.

A. Four-petals Path Tracking

Firstly, a comparison between different values of λ is presented. In section II, we have discussed this drift-free criterion, where $\lambda = 0$ denotes no consideration of drift-free and $\lambda = 4$ (or another nonzero value) is converse. In this comparative simulation, the RMP (11)-(13) is solved by 94LVI method (22), and the execution time for once whole path tracking is set as $T = 15$s. The results are showed in Fig. 2. It is obvious that every joint of PUMA560 can return to the initial state while taking the drift-free criterion into consideration, hence it is an important precondition for repetitive motion planning.

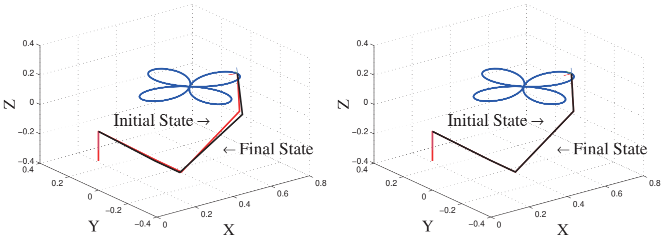

(a) (b)

Fig. 2. Simulative results of drift-free criterion in four-petals path tracking. (a) $\lambda = 0$. (b) $\lambda = 4$.

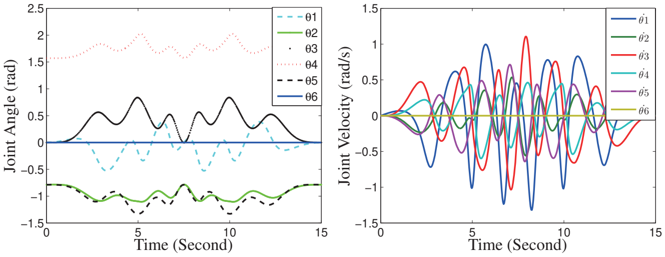

(a) (b)

Fig. 3. Joint angles and joint velocities of PUMA560 synthesized by RMP with $\lambda = 4$ and 94LVI method (22) for tracking the four-petals path. (a) Joint angles. (b) Joint velocities.

TABLE II
Computer Time (s) of Six Numerical Method for Tracking the Four-Petals Path

#	94LVI	E47	M3	M4	M5	M6
1	12.7033	6.7373	66.6818	12.1739	43.2422	10.2233
2	12.9577	6.6513	66.5541	12.4580	43.3659	9.2305
3	12.6965	6.5839	66.2483	12.2679	43.1694	10.1234
4	12.7099	6.3853	65.8536	12.2377	43.1647	9.9262
5	12.6709	6.4012	66.1385	12.4111	43.1489	10.3983

Secondly, Fig. 3 reveals joint angles and joint velocities of PUMA560 during the whole tracking process. By contrasting to Table I, we find that there are no joints exceed physical limits, and joint velocities are at the range of $[-1.5, 1.5]$ (rad/s).

Thirdly, we employ all the six numerical methods to solve PLPE (20) as well as RMP (11)-(13). The compute time, joint drift and end-effector position error in the complex closed path tracking process are presented and analyzed. The compute time of all the six numerical methods are listed in Table II. Note that E47 method (23) costs the least time, while M3 method (24) costs the most. 94LVI, M4 and M6 methods also have a considerable computation speed. Table III shows the joint drift between initial state and final state. As can be seen from Table III, every joint drift of PUMA560 is less than 10^{-5} (rad). Hence, it is reasonable to say that all the six numerical methods can plan the repetitive motion for redundant robot manipulators.

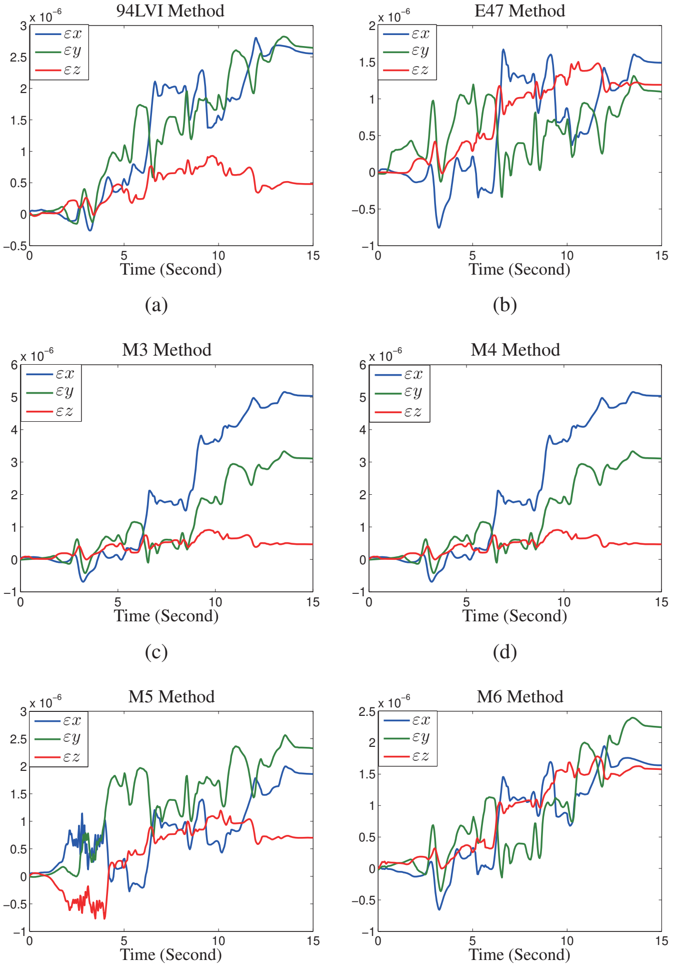

(a) (b) (c) (d) (e) (f)

Fig. 4. The end-effector position errors of PUMA560 synthesized by all the six numerical methods. (a) 94LVI. (b) E47. (c) M3. (d) M4. (e) M5. (f) M6.

Moreover, Fig. 4 shows the end-effector position error of each numerical method, which is defined as $\varepsilon = r - f(\theta)$; ε_x, ε_y and ε_z denote the error in X, Y and Z direction, respectively. From Fig. 4, we notice that for each numerical method the end-effector position error is less than 10^{-5} (m), and thus we can conclude that all the six numerical methods can effectively solve RMP (11)-(13) for redundant robot of manipulators.

B. Five-pointed-star Path Tracking

Similar to simulation of four-petals path tracking, we also analyze the compute time, joint drift and end-effector position error in five-pointed-star path tracking.

Firstly, Fig. 5 demonstrates joint angles and joint velocities of PUMA560 during the whole five-pointed path tracking process. By contrasting to Table I, simulation result shows that joint angles and joint velocities are at feasible ranges.

Secondly, the comparison of compute time among the six numerical methods is presented in Table V. Similarly, E47 method (23) costs the least time of computation. 94LVI, M4 and M6 methods also have good performance, while M3 and

TABLE III

Joint Drifts (m) of Six Numerical Methods for Tracking the Four-Petals Path

Joint-drift	94LVI	E47	M3	M4	M5	M6
$\theta_1(15) - \theta_1(0)$	-5.0160×10^{-6}	-2.8086×10^{-6}	-6.3589×10^{-6}	-4.3697×10^{-6}	-4.4284×10^{-6}	-4.3840×10^{-6}
$\theta_2(15) - \theta_2(0)$	-2.3883×10^{-6}	-1.8801×10^{-6}	-5.3472×10^{-6}	-5.0057×10^{-6}	-1.8268×10^{-6}	-2.7357×10^{-6}
$\theta_3(15) - \theta_3(0)$	-2.1117×10^{-6}	-4.5231×10^{-6}	3.2700×10^{-6}	-3.0729×10^{-6}	-3.6114×10^{-6}	-3.9413×10^{-6}
$\theta_4(15) - \theta_4(0)$	-2.3928×10^{-6}	2.3173×10^{-6}	2.5634×10^{-5}	2.4521×10^{-5}	2.3452×10^{-6}	2.3366×10^{-5}
$\theta_5(15) - \theta_5(0)$	-6.2540×10^{-6}	5.6179×10^{-6}	-9.2761×10^{-6}	-8.1923×10^{-6}	-5.5667×10^{-6}	-5.8205×10^{-6}
$\theta_6(15) - \theta_6(0)$	0	0	0	0	0	0
$\|\theta(15) - \theta(0)\|_2$	2.5436×10^{-5}	2.4504×10^{-6}	2.8686×10^{-6}	2.6695×10^{-5}	2.4839×10^{-5}	-2.4941×10^{-5}

TABLE IV

Joint Drifts (m) of Six Numerical Methods for Tracking the Five-Pointed-Star Path

Joint drift	94LVI	E47	M3	M4	M5	M6
$\theta_1(15) - \theta_1(0)$	6.0699×10^{-6}	1.2740×10^{-5}	1.3497×10^{-5}	1.1264×10^{-5}	1.0313×10^{-5}	6.3533×10^{-6}
$\theta_2(15) - \theta_2(0)$	-7.1712×10^{-6}	-1.9946×10^{-5}	-1.9219×10^{-5}	-1.8383×10^{-5}	-1.9629×10^{-5}	-9.3808×10^{-6}
$\theta_3(15) - \theta_3(0)$	-3.3858×10^{-5}	-6.8786×10^{-5}	6.9262×10^{-5}	-7.1534×10^{-5}	-6.9258×10^{-5}	-3.2785×10^{-5}
$\theta_4(15) - \theta_4(0)$	1.4662×10^{-4}	3.0442×10^{-4}	3.0425×10^{-4}	3.0352×10^{-4}	3.0426×10^{-4}	1.4699×10^{-4}
$\theta_5(15) - \theta_5(0)$	2.2988×10^{-5}	5.0995×10^{-5}	5.1306×10^{-5}	5.3095×10^{-5}	5.1891×10^{-5}	2.1713×10^{-5}
$\theta_6(15) - \theta_6(0)$	0	0	0	0	0	0
$\|\theta(15) - \theta(0)\|_2$	1.5254×10^{-4}	3.1711×10^{-4}	3.1709×10^{-4}	3.1706×10^{-4}	3.1171×10^{-4}	1.5259×10^{-4}

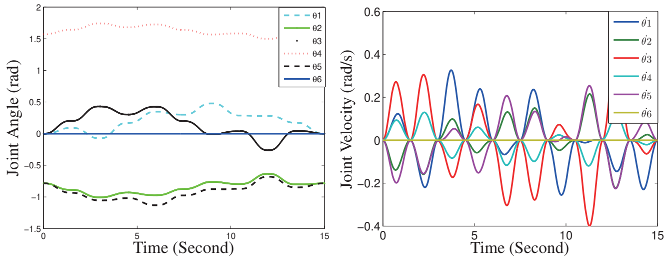

(a)

(b)

Fig. 5. Joint angles and joint velocities of PUMA560 synthesized by RMP with $\lambda = 4$ and 94LVI method (22) for tracking the five-pointed-star path. (a) Joint angles. (b) Joint velocities.

TABLE V

Compute Time (s) of Six Numerical Methods for Tracking the Five-Pointed-Star Path

#	94LVI	E47	M3	M4	M5	M6
1	13.6875	8.8499	65.5533	11.0472	39.3510	12.3424
2	13.0835	8.8451	65.9408	11.3323	39.2237	12.0653
3	12.9111	9.1316	65.5894	11.6565	38.8590	12.0275
4	13.2046	9.0251	65.8957	11.8247	38.9912	11.6947
5	13.2639	9.0084	65.8150	11.1456	39.0178	11.9011

M5 methods cost more time in computation relatively. Table IV shows joint drift of PUMA560 between initial state and final state. Note that all the joint drift are less than 10^{-4} (rad), that is to say, all the six numerical methods can complete the repetitive motion planning in five-pointed-star path tracking. As can be seen from Fig. 6, the end-effector position error of PUMA560 in five-pointed star tracking process solved by all the six numerical methods are less than 6×10^{-6} (m), The simulation results verify the effectiveness of all the six numerical methods to solve RMP (11)-(13) for redundant robot manipulators.

In summary, from the four-petals path and five-pointed-star path tracking simulations, we can draw the conclusion that all the aforementioned six numerical methods can complete RMP (11)-(13) for redundant robot manipulators with considerable accuracy. What is more, 94LVI, E47, M4 and M6 methods have faster computation time than M3 and M5 methods.

VI. Conclusion

In this paper, three novel numerical methods have been designed, investigated and analyzed to plan repetitive motion of redundant robot manipulators. Without loss of generality, the global convergence property of M5 method has been theoretically proved, and that of M3 and M6 methods has been analyzed by computer simulations. Furthermore, associating with three traditional methods, the computation time, joint-drifts and end-effector position errors among all the six numerical methods have been demonstrated and compared. Simulation results have verified that all the six numerical methods can complete the complex closed cyclic motion planning mission with nice accuracies.

Our future work is to summarize and compare the practical application results of several existing neural network methods and numerical methods for solving kinematics resolution problems of redundant robot manipulators, and try to optimize these algorithms.

References

[1] Y. Zhang, Z. Tan, K. Chen, Z. Yang, and X. Lv, "Repetitive motion of redundant robots planned by three kinds of recurrent neural networks and illustrated with a four-link planar manipulators straight-line example," *Robotics and Autonomous Systems*, vol. 57, no. 6, pp. 645–651, 2009.

[2] Y. Zhang, J. Wang, and Y. Xia, "A dual neural network for redundancy resolution of kinematically redundant manipulators subject to joint limits and joint velocity limits," *IEEE transactions on Neural Networks*, vol. 14, no. 3, pp. 658–667, 2003.

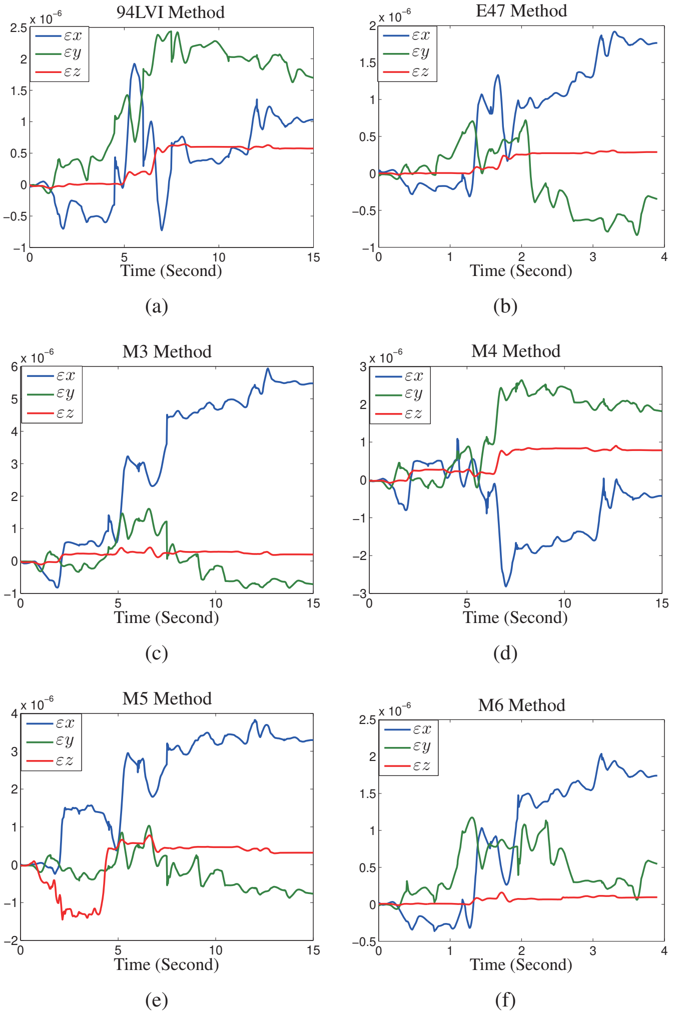

(a) (b)

(c) (d)

(e) (f)

Fig. 6. The end-effector position errors of PUMA560 synthesized by all the six numerical methods. (a) 94LVI. (b) E47. (c) M3. (d) M4. (e) M5. (f) M6.

[3] G. S. Chyan and S. Ponnambalam, "Obstacle avoidance control of redundant robots using variants of particle swarm optimization," *Robotics and Computer-Integrated Manufacturing*, vol. 28, no. 2, pp. 147–153, 2012.

[4] M. Jin, C. Zhou, and Y. Liu, "Hybrid impedance control of 7-dof redundant manipulator with dual compliant surface," in *IEEE International Conference on Mechatronics and Automation*, pp. 1424–1429, IEEE, 2015.

[5] S. Ma, I. Kobayashi, S. Hirose, and K. Yokoshima, "Control of a multijoint manipulator moray arm," *IEEE/ASME Transactions on Mechatronics*, vol. 7, no. 3, pp. 304–317, 2002.

[6] E. Zergeroglu, D. D. Dawson, I. W. Walker, and P. Setlur, "Nonlinear tracking control of kinematically redundant robot manipulators," *IEEE/ASME Transactions on Mechatronics*, vol. 9, no. 1, pp. 129–132, 2004.

[7] S. F. Assal, K. Watanabe, and K. Izumi, "Neural network-based kinematic inversion of industrial redundant robots using cooperative fuzzy hint for the joint limits avoidance," *IEEE/ASME Transactions on Mechatronics*, vol. 11, no. 5, pp. 593–603, 2006.

[8] L. Jin, S. Li, L. Xiao, R. Lu, and B. Liao, "Cooperative motion generation in a distributed network of redundant robot manipulators with noises," *IEEE Transactions on Systems, Man, & Cybernetics: Systems*, vol. 48, no. 10, pp. 1715–1724, 2017.

[9] T. T. C. Kim B S, Li J, "Two-parameter robust repetitive control with application to a novel dual-stage actuator for noncircular machining," *IEEE/ASME Transactions on Mechatronics*, vol. 9, no. 4, pp. 644–652, 2004.

[10] J. J. Craig, "Introduction to robotics - mechanics and control," *Automatica*, vol. 23, no. 2, pp. 263–264, 2005.

[11] C. A. Klein and C.-H. Huang, "Review of pseudoinverse control for use with kinematically redundant manipulators," *IEEE Transactions on Systems, Man, and Cybernetics*, no. 2, pp. 245–250, 1983.

[12] R. V. Mayorga, A. K. C. Wong, and N. Milano, "A fast procedure for manipulator inverse kinematics evaluation and pseudoinverse robustness," *IEEE Transactions on Systems, Man, & Cybernetics*, vol. 22, no. 4, pp. 790–798, 1992.

[13] Z. Zhang, L. Kong, and Y. Niu, "A time-varying-constrained motion generation scheme for humanoid robot arms," in *Advances in Neural Networks - ISNN 2018, Lecture Notes in Computer Science*, vol. 10878, pp. 757–767, Springer, 2018.

[14] Z. Zhang and Y. Zhang, "Equivalence of different-level schemes for repetitive motion planning of redundant robots," *Acta Automatica Sinica*, vol. 39, no. 1, pp. 88–91, 2013.

[15] Y. Zhang, L. Xie, Z. Zhang, K. Li, and L. Xiao, "Real-time joystick control and experiments of redundant manipulators using cosine-based velocity mapping," in *IEEE International Conference on Automation and Logistics*, pp. 345–350, IEEE, 2011.

[16] Y. Zhang, J. Li, M. Mao, W. Li, and S. Fu, "Complete theory for e47 and 94lvi algorithms solving inequality-and-bound constrained quadratic program efficiently," in *Chinese Automation Congress*, pp. 183–189, IEEE, 2015.

[17] Y. Zhang, S. S. Ge, and T. H. Lee, "A unified quadratic-programming-based dynamical system approach to joint torque optimization of physically constrained redundant manipulators," *IEEE Transactions on Systems, Man, & Cybernetics: Cybernetics*, vol. 34, no. 5, pp. 2126–2132, 2004.

[18] Z. Zhang, L. Kong, L. Zheng, P. Zhang, X. Qu, B. Liao, and Z. Yu, "Robustness analysis of a power-type varying-parameter recurrent neural network for solving time-varying qm and qp problems and applications," *IEEE Transactions on Systems, Man, & Cybernetics: Systems*, vol. PP, no. 99, pp. 1–14, 2018. DOI: 10.1109/TSMC.2018.2866843.

[19] Y. Xia, "A new neural network for solving linear programming problems and its application," *IEEE Transactions on Neural Networks*, vol. 7, no. 2, pp. 525–529, 1996.

[20] Y. Zhang, Y. Yang, N. Tan, and B. Cai, "Zhang neural network solving for time-varying full-rank matrix moore–penrose inverse," *Computing*, vol. 92, no. 2, pp. 97–121, 2011.

[21] L. Jin and Y. Zhang, "G2-type srmpc scheme for synchronous manipulation of two redundant robot arms," *IEEE Transactions on Cybernetics*, vol. 45, no. 2, pp. 153–164, 2017.

[22] B. He, "A new method for a class of linear variational inequalities," *Mathematical Programming*, vol. 66, no. 1-3, pp. 137–144, 1994.

[23] Z. Zhang and Y. Zhang, "Variable joint-velocity limits of redundant robot manipulators handled by quadratic programming," *IEEE/ASME Transactions on Mechatronics*, vol. 18, no. 2, pp. 674–686, 2013.

[24] B. He, "Solving a class of linear projection equations," *Numerische Mathematik*, vol. 68, no. 1, pp. 71–80, 1994.

[25] Z. Zhang, L. Zheng, J. Yu, Y. Li, and Z. Yu, "Three recurrent neural networks and three numerical methods for solving a repetitive motion planning scheme of redundant robot manipulators," *IEEE/ASME Transactions on Mechatronics*, vol. 22, no. 3, pp. 1423–1434, 2017.

[26] C. A. Klein and K. B. Kee, "The nature of drift in pseudoinverse control of kinematically redundant manipulators," *IEEE Transactions on Robotics and Automation*, vol. 5, no. 2, pp. 231–234, 1989.

[27] L. Xiao and Y. Zhang, "Acceleration-level repetitive motion planning and its experimental verification on a six-link planar robot manipulator," *IEEE Transactions on Control Systems Technology*, vol. 21, no. 3, pp. 906–914, 2013.

[28] Y. Z. Zhang Y, Tan Z, "A dual neural network applied to drift-free resolution of five-link planar robot arm," *International Conference on Information and Automation*, pp. 1274 – 1279, 2008.

[29] Boyd, Vandenberghe, and Faybusovich, "Convex optimization," *IEEE Transactions on Automatic Control*, vol. 51, no. 11, pp. 1859–1859, 2006.

[30] Y. Zhang and J. Wang, "A dual neural network for convex quadratic programming subject to linear equality and inequality constraints," *Phys. Lett*, vol. 298, no. 4, pp. 271–278, 2002.